Substrate Tolerant Direct Block Copolymer Nanolithography[†]

Tao Li,[a] Zhongli Wang,[ab] Lars Schulte,[ab] and Sokol Ndoni*[ab]

[a]Department of Micro- and Nanotechnology, Technical University of Denmark,

DK-2800 Kgs. Lyngby, Denmark.

[b]Center for Nanostructured Graphene (CNG), Technical University of Denmark, DK-2800 Kgs. Lyngby, Denmark.

*To whom correspondence should be addressed. E-mail: sond@nanotech.dtu.dk (S. N.)

[†]Electronic supplementary information (ESI) available: Experimental section, additional figures and tables.

Abstract : Block copolymer (BC) self-assembly constitutes a powerful platform for nanolithography. However, there is a need for a general approach to BC lithography that critically considers all the steps from substrate preparation to the final pattern transfer. We present a procedure that significantly simplifies the main stream BC lithography process, showing a broad substrate tolerance and allowing for efficient pattern transfer over wafer scale. PDMS-rich poly(styrene-b-dimethylsiloxane) (PS-b-PDMS) copolymers are directly applied on substrates including polymers, silicon and graphene. A single oxygen plasma treatment enables formation of the oxidized PDMS hard mask, PS block removal and polymers or graphene substrate patterning.
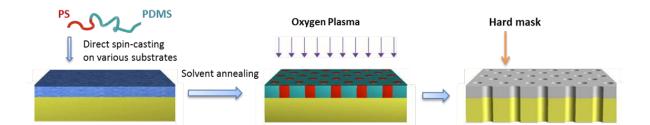
Main Text:

The ever growing demand for increased device functionality, higher data processing speed and larger data storage density drives the searching for new technology to fabricate electronic components with smaller dimensions. BC lithography is a promising platform to meet the key challenges of small feature size with high resolution and high throughput at low cost.[1, 2] The domain size can be controlled in the range of 5-50 nm by controlling molecular weight of the BC and the segregation strength between the blocks in the synthesis step. Several morphologies including spheres, lamellas and cylinders, have been explored for nanolithography application.[3] BCs combining high intrinsic immiscibility (quantified by a high Flory-Huggins interaction parameter χ) with high etching contrast are extremely attractive as precursors for nanolithographic masks.[4] PS-b-PDMS (SD) has $\chi_{SD} \sim 0.27$ at room T, and can easily self-assemble into morphologies with sub-10 nm features.[5, 6] Under oxygen plasma the PDMS block is oxidized into hard and thermally stable silicon oxy carbide, which acts as the effective lithographic mask, while the PS block is efficiently degraded.[7] These two features have gained

2

SD intense research interest in the last decade. However, the orientation control of SD is notoriously challenging due to the large surface energy mismatch between the blocks.[8] As a result a top wetting layer of PDMS preferably forms at the SD-air interface. A brush layer is routinely applied to prevent dewetting and a top-coat or sophisticated annealing conditions,[9] are used for orientation control.

   The present contribution is motivated by the great interest in SD for nanolithography, with a focus on even more challenging and rarely reported PDMS-rich BCs, which are equally, if not more, important for pattern transfer process.[10] The BC film is applied directly on the substrate, thus bypassing the step of initial substrate surface modification found in nearly all the reports in the field. The preliminary surface modification, including the grafting of a neutral polymer brush layer onto the substrate,[11] is the result of thinking thin film BC self-assembly in terms of equilibrium. Uneven BC swelling under selective solvent vapor is known to shift the morphology by changing the effective volume fraction,[12, 13] which opens up the process window for capturing the targeted morphology kinetically. The lithography process is schematically illustrated in Scheme 1 and proved valid for a number of substrates with widely varying surface energies. To our best knowledge, this is the first report on highly ordered PDMS-rich BC masks with perpendicular cylindrical orientation, which shows unparalleled simplicity and applicability in block copolymer nanolithography.

Scheme 1. Schematic workflow of direct BCs nanolithography: SDs in heptane are directly cast on various substrates including PS, polylactide (PLA), poly(methyl methacrylate) (PMMA), polysulfone (PSF), cross-linked 1,2-polybutadiene (PB), graphene and silicon.

Four SDs with different number-average molecular weights (M_n) from 23.4 to 67.0 kg/mol are investigated (Table S1, supporting information). The PS volume fraction is in the range of 24-30%, which is within the typical composition range for cylinder bulk morphology (Figure S1, supporting information). SD23, SD34 and SD42 are synthesized in our lab by living anionic polymerization[14] with a narrow polydispersity index (PDI ≤ 1.03), and SD67 is purchased with somewhat higher PDI (1.45). SD solutions in heptane are spin-cast into sub-20 nm thin films on silicon and a number of common polymer substrates. Heptane is a nonsolvent for these polymer substrates, allowing direct spin-casting of the SD without any disturbance. Figures 1a,b,c show top view scanning electron microscopy (SEM) images of SD23, SD34 and SD42 after annealing. A well-ordered hexagonally packed cylinder morphology with narrow PS-cylinder size distribution is clearly seen, which can be visualized directly in SEM. A SEM image of SD67 after annealing (Figure S2, supporting information), shows the same morphology but lacking in lateral order, which might be due to its large PDI. Compared with the morphology of as cast films or of films after thermal annealing (Figure S3a,b, supporting informarion), it is evident that the solvent annealing is effective on directing the SD self-assembly over large areas (2 inch wafer tested) with micrometer grain size (Figure S3c). The corresponding period (Table. S1)

scales with the 0.6^{th} power of BC molecular weights. A wide range of the pore size from 13 nm

(SD23) to 30 nm (SD67) is obtained. General shortcomings of solvent vapor annealing,

including dewetting and deformation of the structures,[15] are not observed in this study due to the

limited PS chain mobility in the presence of a nonsolvent. The morphology is further confirmed

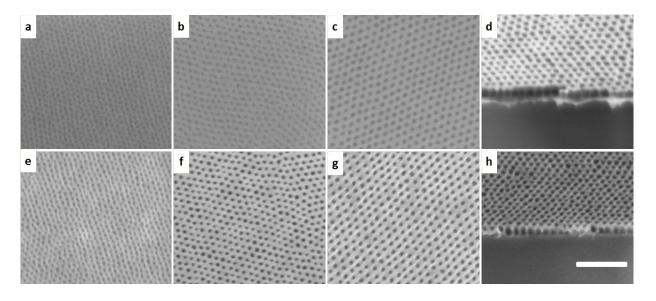by atomic force microscopy (AFM) (Figure S4, supporting information).

Figure 1. (a-c) Top view SEM images of the masks on PS after annealing: (a) SD23 annealed in

2, 2, 4-trimethylpentane (TMPA) for 40 minutes, (b) SD34 annealed in 2, 4, 4-trimethyl-1-

pentene (TMPE) for 30 minutes, and (c) SD42 annealed in hexane for 40 minutes. (e-g) Top

view SEM images of the masks on PS after pattern transfer: (e) SD23 and (f) SD34 after SF_6 and

O_2 plasma etching, and (g) SD42 after O_2 plasma etching alone. The O_2 reactive ion etching (RIE)

step solidifies the PDMS domain, removes the PS domain and transfers the pattern to the PS

substrate simultaneously. (d and h) Tilted SEM images for the SD42 mask: (d) after etching and

(h) after mask removal. All the samples are spin-cast on a PS 50k substrate coated on silicon

wafer with a thickness of around 50 nm. Scale bar: 200 nm.

The pattern transfer is conducted by RIE (Figure 1e, f, g). In most cases, a short SF_6 RIE is firstly used to remove a thin layer of residual PDMS on top. The improved SEM image contrast after etching suggests the successful pattern transfer, which is further evidenced by the cross-section image of the samples after etching (Figure 1d, h). The mask can be readily removed by a SF_6 RIE (confirmed by the absence of Si element in X-ray photoelectron spectroscopy measurement) without damage to polymer substrate (Figure 1h). Figure S5 (supporting information) shows the SD23 only treated with O_2 RIE and most of the pores stay clogged. However, in some cases (Table S2, supporting information), only an O_2 RIE is sufficient to complete the pattern transfer (Figure 1g). In these cases the film is free of a PDMS top wetting layer after solvent vapor annealing, which is difficult to obtain for PDMS-containing BC. The mask produced has high etching resistance under oxygen plasma and high thermal stability (morphology stays the same after $700^{o}C$ for one hour).

A discussion of the annealing conditions, the time evolution of the structural order and a conjectured mechanism of pattern formation at optimum and post-optimum annealing conditions can be found in the supporting information (Scheme S1 and Figure S7).

The presented approach also shows strong substrate independence, as demonstrated in Figure 2 and 3 The observed self-assembly behavior is similar to the already discussed behavior on PS substrate for all the tested substrates: PLA, PMMA, PSF, PB, graphene and silicon with native oxide layer (The surface energy of these substrates can be characterized by water contact angle measurement summarized in Table S3). The timing of the morphology evolution is somewhat different in each case but generally faster than the already discussed PS substrate. The pattern transfer is proved successful for all the substrates. Figure 2b shows the cross-section of polysulfone patterned by the SD34 mask; a well-ordered nano-pore channel array is clearly

6

observed. Polysulfone is a technologically relevant material for ultrafiltration membranes due to its high thermal, mechanical and chemical resistance.[16] For membrane bio-analysis and separation, challenges still exist as to produce reliable membranes with anti-fouling properties, high flux and narrow pore distribution. After oxygen plasma etching, the iso-porous PSF membrane becomes hydrophilic (water contact angle: 19°), which may significantly improve its anti-fouling properties.[17, 18] The demonstrated pattern transfer could offer an alternative solution to manufacture high performance thin polymer membranes.
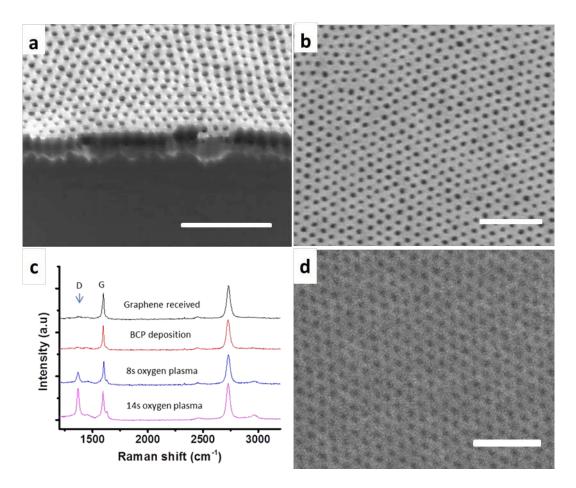

Figure 2. SEM images of pattern transfer to polysulfone and graphene. (a) Tilted and (b) top views of polysulfone patterned by SD34. (c) Raman spectrum characterization of graphene

patterning in the presence of the mask from SD42 and (d) top-view SEM image of the graphene

nanomesh patterned by SD42. Scale bars: 200nm.

This method is also particularly suitable for patterning of two-dimensional materials where part

of the single atom layer is removed in a controlled way to give tunable properties. Graphene

nanomesh is a typical example, in which high-density arrays of nanoscale holes are punched.[19]

The available BC lithography for graphene nanomesh is tedious, involving multiple deposition

and etching steps.[20] Most of all, it is difficult to reach sub-30 nm periods with the low-χ PS-

PMMA mask used in most reports. Here, SD is directly deposited on CVD-grown single layer

graphene. Figure S6 (supporting information) shows large-area mask covering graphene without

defects after solvent annealing. The pattern is well adjusted on grain boundaries, multi-layer

islands and substrate defects. We use Raman spectroscopy to analyze the hole punching process.

After the BC deposition, the spectrum stays the same. Increase in oxygen plasma etching time

results in the increase of D peak, which typically characterizes the hole enlarging process. The

excellent process control is evidenced by the essentially unchanged width of the G peak. Figure

2d shows the patterned graphene after removing part of the mask by scotch tape; the image

shows a high fidelity reproduction of the mask morphology. The obtained graphene nanomesh

has potentially many important applications, including fabrication of field-effect transistors,[21]

gas sensors,[22] and atomic-layer separation membranes.[23]

The oxidized PDMS masks can be used not only for patterning carbonaceous materials by

oxygen RIE; they also show higher resistance over silicon under chlorine RIE as demonstrated

by the SEM images in Figures 3a,b. Unlike the isotropic fluorine plasma etching, where the pore-

broadening is significant (see fig. 3c,d), the silicon etching by chlorine plasma is highly

anisotropic.[24] Therefore, regular arrays of high-aspect-ratio holes in silicon are obtained by direct

application of chlorine plasma to the oxidized PDMS mask. This process can be applied to pattern silicon with other morphologies, such as lines and dots by PDMS-based BC masks, which is of great relevance for semiconductor industry and solid-state nanoporous materials. [25]
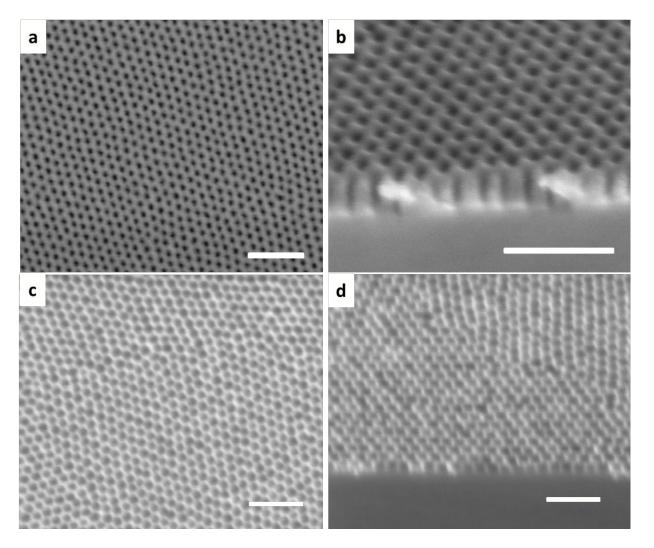

Figure 3. SEM image of a) top-view and b) cross-section of the silicon patterned by chlorine RIE. Holes with aspect ratio exceeding 4 are clearly visible in b). c) top-view and d) cross-section of the silicon patterned by SF_6 plasma etching. Several fluorine based RIE recipes including Bosch process have been tested. Scale bars: 200 nm.

In conclusion, we have demonstrated a novel design for BC thin film morphology control, which significantly simplifies the nanolithography pattern transfer process on polymer substrates, graphene and silicon, opening up for numerous potential applications. This conceptual approach provides a powerful toolset to obtain desired BC mask morphologies, which are difficult to realize by conventional methods.

Author Contributions

T.L. conceived and designed the experiments. T.L., Z.W. and L.S. performed the experiments. T.L and S.N analyzed the data. L.S. synthesized and characterized the block copolymers. T.L. and S.N co-wrote the paper. S.N. supervised the project. All the authors discussed the results and corrected the manuscript. All authors have given approval to the final version of the manuscript.

Funding Sources

REFERENCES

1. C. M. Bates, M. J. Maher, D. W. Janes, C. J. Ellison and C. G. Willson, *Macromolecules*, 2014, **47**, 2-12.
2. J. Bang, U. Jeong, D. Y. Ryu, T. P. Russell and C. J. Hawker, *Adv Mater*, 2009, **21**, 4769-4792.
3. X. D. Gu, I. Gunkel and T. P. Russell, *Philos T R Soc A*, 2013, **371**.
4. A. Nunns, J. Gwyther and I. Manners, *Polymer*, 2013, **54**, 1269-1284.
5. Y. S. Jung and C. A. Ross, *Nano Lett*, 2007, **7**, 2046-2050.
6. T. Nose, *Polymer*, 1995, **36**, 2243-2248.

7.   K. Fukukawa, L. Zhu, P. Gopalan, M. Ueda and S. Yang, *Macromolecules*, 2005, **38**, 263-270.
8.   E. Kim, W. Kim, K. H. Lee, C. A. Ross and J. G. Son, *Adv Funct Mater*, 2014, **24**, 6981-6988.
9.   K. W. Gotrik, A. F. Hannon, J. G. Son, B. Keller, A. Alexander-Katz and C. A. Ross, *Acs Nano*, 2012, **6**, 8052-8059.
10.   C. C. Chao, T. C. Wang, R. M. Ho, P. Georgopanos, A. Avgeropoulos and E. L. Thomas, *Acs Nano*, 2010, **4**, 2088-2094.
11.   M. Park, C. Harrison, P. M. Chaikin, R. A. Register and D. H. Adamson, *Science*, 1997, **276**, 1401-1404.
12.   W. B. Bai, A. F. Hannon, K. W. Gotrik, H. K. Choi, K. Aissou, G. Liontos, K. Ntetsikas, A. Alexander-Katz, A. Avgeropoulos and C. A. Ross, *Macromolecules*, 2014, **47**, 6000-6008.
13.   T. Y. Lo, C. C. Chao, R. M. Ho, P. Georgopanos, A. Avgeropoulos and E. L. Thomas, *Macromolecules*, 2013, **46**, 7513-7524.
14.   S. Ndoni, P. Jannasch, N. B. Larsen and K. Almdal, *Langmuir*, 1999, **15**, 3859-3865.
15.   M. Y. Paik, J. K. Bosworth, D. M. Smilges, E. L. Schwartz, X. Andre and C. K. Ober, *Macromolecules*, 2010, **43**, 4253-4260.
16.   B. S. Lalia, V. Kochkodan, R. Hashaikeh and N. Hilal, *Desalination*, 2013, **326**, 77-95.
17.   K. S. Kim, K. H. Lee, K. Cho and C. E. Park, *J Membrane Sci*, 2002, **199**, 135-145.
18.   M. L. Steen, L. Hymas, E. D. Havey, N. E. Capps, D. G. Castner and E. R. Fisher, *J Membrane Sci*, 2001, **188**, 97-114.
19.   J. Yang, M. Z. Ma, L. Q. Li, Y. F. Zhang, W. Huang and X. C. Dong, *Nanoscale*, 2014, **6**, 13301-13313.
20.   J. W. Bai, X. Zhong, S. Jiang, Y. Huang and X. F. Duan, *Nat Nanotechnol*, 2010, **5**, 190-194.
21.   J. G. Son, M. Son, K. J. Moon, B. H. Lee, J. M. Myoung, M. S. Strano, M. H. Ham and C. A. Ross, *Adv Mater*, 2013, **25**, 4723-4728.
22.   A. Cagliani, D. M. A. Mackenzie, L. K. Tschammer, F. Pizzocchero, K. Almdal and P. Boggild, *Nano Res*, 2014, **7**, 743-754.
23.   K. Celebi, J. Buchheim, R. M. Wyss, A. Droudian, P. Gasser, I. Shorubalko, J. I. Kye, C. Lee and H. G. Park, *Science*, 2014, **344**, 289-292.
24.   K. R. Williams and R. S. Muller, *J Microelectromech S*, 1996, **5**, 256-269.
25.   B. N. Miles, A. P. Ivanov, K. A. Wilson, F. Dogan, D. Japrung and J. B. Edel, *Chem Soc Rev*, 2013, **42**, 15-28.